Mapping antibonding electron states of a Pb adatom on Pb(111)

J. C. Lian,[1] Z. H. Cheng,[1] Y. H. Jiang,[1] Y. Y. Zhang,[1] L. W. Liu,[1] W. Ji,[1] W. D. Xiao,[1] S. X. Du,[1] W. A. Hofer,[2] and H.-J. Gao[1,*]

[1]*Institute of Physics, Chinese Academy of Sciences, Beijing 100190, China*

[2]*Surface Science Research Center, The University of Liverpool, Liverpool L69 3BX, United Kingdom*

(Received 22 November 2009; revised manuscript received 25 March 2010; published 7 May 2010)

We have used low-temperature scanning tunneling spectroscopy to spatially map the energy-resolved electron density of a single Pb adatom on a Pb(111) surface. We observe a clear spatial inhomogeneity of the spectral density of the Pb adatom. This spatial inhomogeneity is rotated with bias voltage, reflecting the modification of the structure and symmetry of the adatom orbitals by the substrate. The simulated spectral maps of the Pb adatom based on density-functional-theory calculations agree well with experimental observations. This spatial inhomogeneity originates from the local extension of antibonding Pb states and the coupling to the substrate.

DOI: 10.1103/PhysRevB.81.195411 PACS number(s): 68.37.Ef, 73.20.−r, 71.15.−m

I. INTRODUCTIONS

The presence of defects on a surface, such as single atoms, vacancies, and artificial nanostructures, as well as their interaction with the substrate is one of the central topics in surface physics. Understanding the electronic properties of the surface defects is of high interest in a large class fundamental and technological problems ranging from superconductors to heterogeneous catalysis.[1–10] The development of scanning tunneling microscopy (STM) has enabled us to address these issues at the single-atom level, owing to the very high spatial resolution of this technique.[11–13] In recent years STM images in combination with scanning tunneling spectroscopy (STS) have been used to probe the interaction of adatoms with surfaces, e.g., Kondo resonances induced by magnetic adatoms, local effect of magnetic impurities on superconductivity, adatom-induced localization of surface states, and spin electronics.[1–7,14–22] Nilius *et al.*[23] recently explored the influence of the Al_2O_3/NiAl(110) substrate, in particular, the local defects of the Al_2O_3 surface, on the electronic properties of single Pd adatoms. Bound states induced by magnetic adatoms in the superconducting gap of Nb(110) single crystals[4] and Pb thin films[7] were investigated by STS at sub-Kelvin temperature. However, to the best of our knowledge, the *intrinsic* electronic structures of homogeneous adatoms on superconducting metal surfaces have never been reported.

Here, we report on spatially resolved spectroscopic maps of the electronic states of single Pb adatoms modified by their adsorption on a Pb(111) substrate. *In situ* ultrahigh vacuum (UHV) low-temperature (LT) STM measurements reveal asymmetric features in the spectral density of unoccupied states that are rotated with bias voltage, reflecting the structure and symmetry of Pb orbitals influenced by the substrate. Density-functional-theory (DFT) calculations show that this spatial inhomogeneity originates from the local extension of antibonding Pb states and their coupling to the substrate.

II. EXPERIMENTAL AND THEORY

Experiments were carried out in an UHV LT-STM system (Unisoku) equipped with standard surface preparation facilities. The clean Pb(111) surface was prepared by repeated cycles of sputtering with argon ions and annealing. STM images were acquired in constant-current mode and all given voltages are referred to the sample. STS and dI/dV mapping were performed with lock-in technique with bias modulation of 10 mV at a frequency of 991 Hz. All measurements were performed at 4.2 K with mechanically cut Pt-Ir tips, which were further sharpened by controlled collisions with the Pb(111) substrate.

Theoretical calculations were based on density-functional theory, the Perdew-Wang generalized-gradient approximation (GGA) exchange-correlation functional,[24] ultrasoft pseudopotential,[25] and plane waves, as implemented in the VASP code.[26,27] A 400 eV kinetic-energy cutoff and periodic boundary conditions were applied. The minimum-energy lattice constant of Pb in the simulations was 0.507 nm. This is in good agreement with Wei's independent PW-91 GGA calculation which gives 0.504 nm.[28] The adsorption site of a Pb adatom was then determined with two different supercells. To reduce the interaction between the adjacent adatom, one $p(9\times11)$ supercell with three Pb layers was considered initially. Six special k points were used in this simulation to sample the Brillouin zone. Subsequently, the system was mimicked by a $p(3\times3)$ unit cell with five layers. In this simulation we included 12 special k points. In both simulations we find that the ground-state adsorption site is the hollow site; however, both the fcc and hcp hollow sites yielded the same total energy. In all simulations of current contours of spectra we consequently used one site, the fcc hollow site, for comparisons with experiments, checking, however, that the difference between fcc and hcp hollow sites in the transport simulations is negligible.

III. RESULTS AND DISCUSSION

Individual Pb adatoms were created *in situ* by controlled tip-sample contact. This method was based on the same technique used in Rieder's group.[29,30] Large-scale STM images as the one illustrated in Fig. 1(a) show the as-prepared Pb adatoms, as well as small Pb clusters, on the Pb(111) surface. The Pb adatoms on a Pb(111) terrace are imaged as bright

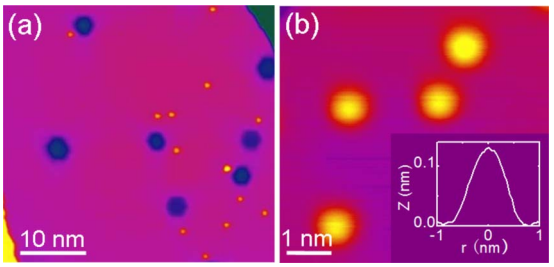

FIG. 1. (Color online) (a) Large-scale topographic image of Pb(111) surface demonstrating Pb adatoms (bright spots) created by controlled tip-sample contact and hexagonal Ar aggregations under the terrace; (b) closeup showing four Pb adatoms on Pb(111) surface; $I=67.3$ pA and $V=-1.5$ V; and inset shows the line profile across an adatom. The apparent height of the adatom is about 0.13 nm and the FWHM is about 0.78 nm.

protrusions with an apparent height of 0.12 ± 0.02 nm. The hexagonal depressions are assigned to subsurface Ar gas bubbles.[31] Figure 1(b) shows a closeup of four Pb adatoms characterized by spherical features with an apparent height of 0.13 nm and a full width at half maximum (FWHM) of 0.78 nm. dI/dV spectra acquired on the Pb adatom and the bare Pb surface are shown in the Fig. 2, respectively. Inset shows the position of the tip where the spectra were measured. The topography images as well as the dI/dV spectra of all the adatoms on the surface (for example, in Fig. 1) are similar. These verify that each atom is identical and of the same element, which is not Pt or Ir but Pb.

Figure 3(a) shows a constant-current STM image of a single Pb adatom. The simultaneously recorded dI/dV images of the same Pb adatom at sample bias values from 0.2 to 1.6 V with an interval of 0.2 V are shown in Figs. 3(b)–3(i). While the constant current contour, which contains a convolution of Pb states over the bias range, is roughly circular, the dI/dV maps clearly show asymmetric features, where single protrusions are accompanied by depressions. With increasing bias voltage a random rotation of the single protrusion with respect to the dark area is observed, in addition to a contrast variation in the single protrusion versus the dark area, as

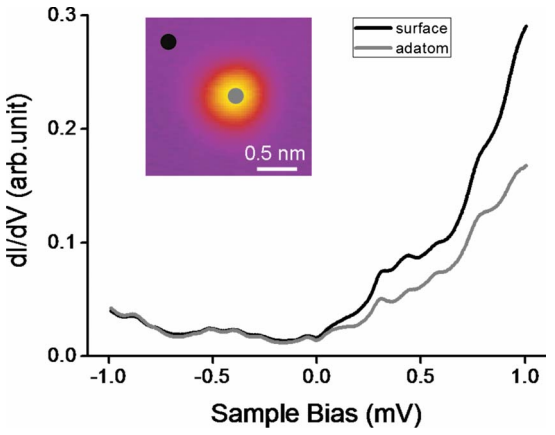

FIG. 2. (Color online) dI/dV spectra acquired on Pb adatom (gray curve) and bare Pb(111) surface (black curve). Inset shows the position of the tip where the spectra were measured.

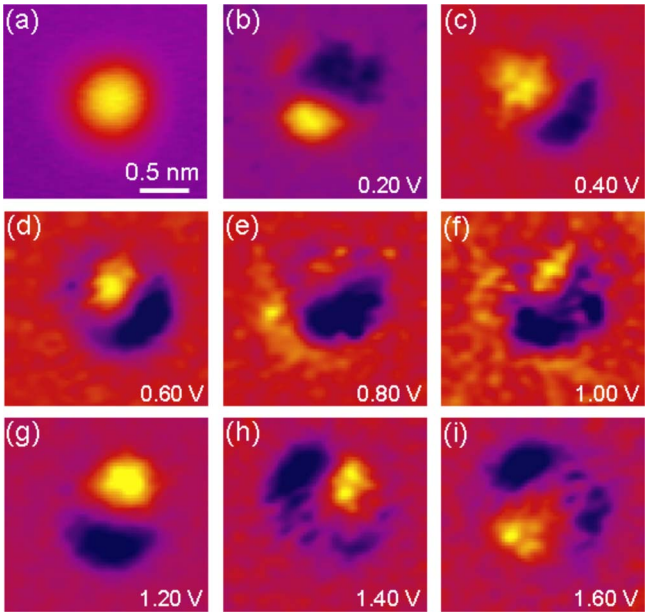

FIG. 3. (Color online) (a) Topographic image of an isolated Pb adatom; $I=0.95$ nA and $V=0.60$ V; [(b)–(i)] dI/dV images of the same area simultaneously acquired with the topography in Fig. 3(a) from 0.20 to 1.60 V with an interval of 0.20 V; and dark to light corresponds to increase in the conductance.

seen in Figs. 3(b)–3(i). The dI/dV mapping represents the density at a distinct narrow energy interval. It is thus related to the square of single-electron wave functions as the sampling voltage in the dI/dV map reaches a limiting value. The dI/dV map then directly shows the spatial variation in these wave functions.[12,13] In positive bias range, it shows the local extension of the density of unoccupied states. Thus, the asymmetric feature in the dI/dV images acquired with positive bias voltages indicates a symmetry breaking in the unoccupied states of the Pb adatom on the Pb(111) surface. We note that one should expect a threefold symmetry of the electronic structure of the Pb adatom on Pb(111) due to the threefold symmetry of the surface. However, this is not, what we observe. Figure 3 clearly shows the absence of any symmetry in the local extension of the density of unoccupied states, indicating that the unoccupied states of the Pb adatom are not hybridizing with the surface density of charge in a simple manner.

In order to exclude the possibility of STM tip artifacts, we have measured dI/dV images of a different Pb adatom with another STM tip, which are shown in Fig. 4. The resolution of this tip is apparently not as good as the tip used above so that a dashed circle is added to demonstrate the contour of the single Pb adatom. Nevertheless, we can still see the asymmetry behavior of the unoccupied states of the Pb adatom on Pb(111) surface from the dI/dV images in positive bias range. Cheng *et al.*[32] observed the similar local density of states (LDOS) asymmetry of the Pb adatom on Pb(111) surface in a separated low-temperature STM system. They manipulated Pb adatoms into a chain and then the dI/dV images were measured within different bias voltages. The LDOS features of each adatoms are different and can be varied with bias. These also confirm that the observed

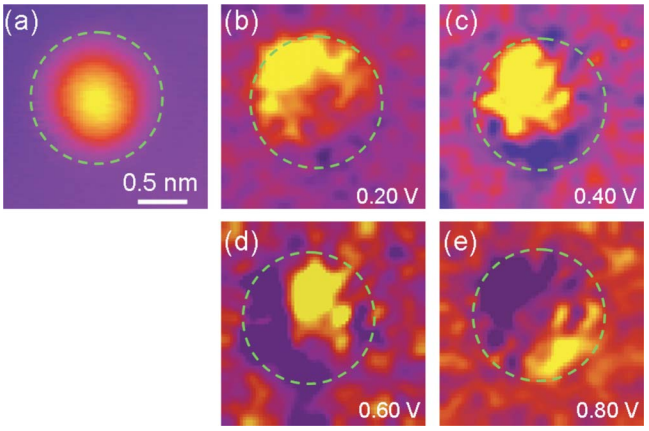

FIG. 4. (Color online) (a) Topographic image of a Pb adatom with a different STM tip; $I=0.30$ nA and $V=0.80$ V, and [(b)–(e)] dI/dV images of the same area simultaneously acquired with the topography in Fig. 4(a) from 0.20 to 0.80 V with an interval of 0.20 V.

strange LDOS features are not induced by the STM tip.

By comparison, the dI/dV images in negative bias voltages range, which depict the local extension of the density of states in occupied energy range, show a different behavior. As seen in Figs. 5(b)–5(f), no significant positional variation is observed for the single protrusion with increasing bias voltage, in contrast to that of the positive bias range, indicating a fundamental difference in the spatial distribution of occupied and unoccupied states of the Pb adatom.

To understand the origin of this surprising effect, we turned to the simulation of current and dI/dV contours. The simulated topographic image of the single adatom is shown in Fig. 6(a).[33,34] The extension of the adatom (more than 1 nm), as well as the apparent height (about 0.15 nm), agree well with the above experimental data. The ground-state configuration of a Pb atom is [Xe] $4f^{14}5d^{10}6s^{2}6p^{2}$. The outermost d electrons are nearly 10 eV below the 6s band (approximately 20 eV below the Fermi level). The electronic properties of Pb are therefore dominated by the 6s and 6p bands, while the 5d levels can be viewed as core levels. In

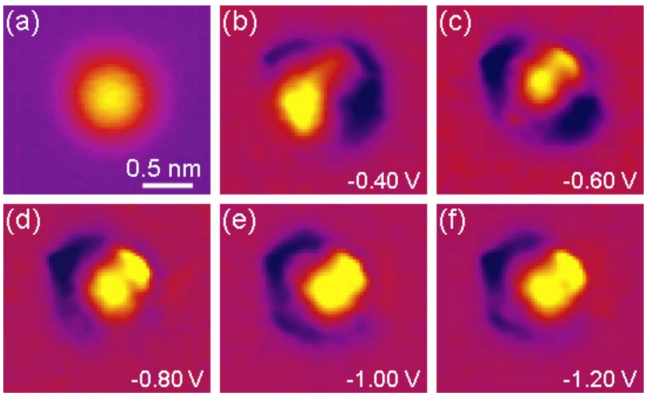

FIG. 5. (Color online) (a) Topographic image of an isolated Pb adatom; $I=1.00$ nA and $V=-1.00$ V; [(b)–(f)] dI/dV images of the same area simultaneously acquired with the topography in Fig. 5(a) from −0.40 to −1.20 V with an interval of 0.20 V.

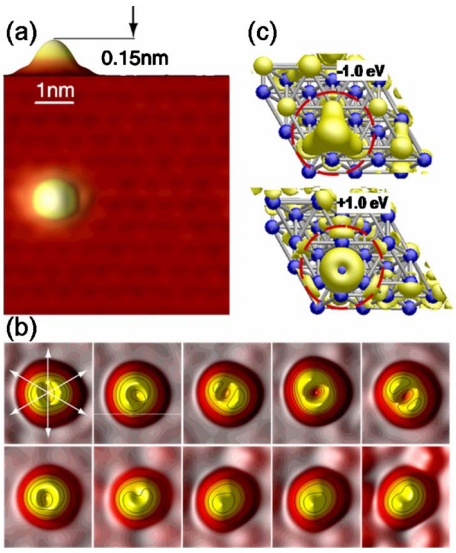

FIG. 6. (Color online) Simulations of a single Pb adatom. (a) Topography of a single Pb adatom in 9×11 unit cell. The extension of the adatom in the scan is larger than 1 nm, the apparent height at $V=1.6$ V is 0.15 nm. Note that the scale in z direction has been increased in the representation. (b) LDOS of a single adatom from 0.2 eV (top left) to 2.0 eV (bottom right) in intervals of 0.2 eV. The spectra show a double feature throughout the energy range, the orientation with respect to the symmetry planes (see arrows) depends on the energy value. (c) Charge-density contour of single states in the negative (−1 V, top) and in the positive (+1 V, bottom) bias regime. Occupied states show a single protrusion into the vacuum while empty states show a ringlike feature. The yellow atoms are the first-layer Pb atoms while the blue ones are the second layer.

this case the Pb adatom may possess sp^3 hybrid atomic orbitals, as, e.g., found for carbon atoms. These hybrid orbitals have a specific orientation and the four lobes are naturally oriented in a tetrahedral fashion. For the unoccupied states, the two orbitals responsible for binding the adatom to the surface cannot be detected by the tip while the other two hybrid atomic orbitals can be seen since they protrude into the vacuum. A systematical analysis of the LDOS confirms the assumption. As shown in Fig. 6(b), the orientation of the LDOS contours, from 0.2 to 2.0 eV above the Fermi level with an interval of 0.2 eV, does not remain constant, but depends on the energy level. It shows two protrusions indicating two hybrid atomic orbitals protruding into the vacuum. In Fig. 6(b), the three equivalent symmetry directions: $[2\bar{1}\bar{1}]$, $[\bar{1}2\bar{1}]$, and $[\bar{1}\bar{1}2]$, are indicated by the white arrows. It is seen that the nodal plane between the two parts of the LDOS contour is rotating with the energy level in a fashion that does not follow the threefold symmetry of the substrate. This is in good agreement with the measured dI/dV images in unoccupied states regime shown in Fig. 3. It is noteworthy that the energy values in the simulations might deviate from those in the experiments, as unoccupied states in DFT calculations do not coincide with excited states of the system. Nevertheless, this well-known deficiency of DFT simulations does not alter the main result.

In negative bias range only one single centered protrusion is detected and does not rotate with bias voltages, as shown

in Fig. 5. The origin of this behavior is shown in Fig. 6(c). Occupied states (−1 eV, top) are bonding states and possess a tetrahedral structure with three lobes pointing in the direction of the surface atom. The fourth lobe, pointing into the vacuum, is detected by tunneling spectroscopy. On the contrary, states in the unoccupied range are antibonding and the density is consequently located at the position of the adatom itself and consists of a two-parts or ringlike structure, parallel to the surface plane.

One may argue that the wavelike feature of the LDOS contour might be nationalized by the interference of the surface state electrons with some defects on the surfaces.[1–3,35,36] However, to the best of our knowledge, no report concerning the surface state on Pb(111) is found in literature, unlike the Shockley surface states of Au(111), Ag(111), and Cu(111). We never observe any standing wave pattern around the Pb adatoms, steps or the Ar bubbles either in large scale STM images or in the dI/dV images. In addition, the oscillatory character of the interaction is related to half of the Fermi wavelength, which is about 3.8 nm in the case of Ag(111) surface, for instance.[30,37] This apparently exceeds the dimension of single Pb adatom, of about 0.8 nm. Thus, the possibilities of the spatial inhomogeneity arising from the interaction with standing wave can be excluded.

IV. SUMMARY

We have measured the energy-resolved spectroscopic mapping of the sp^3 hybridization of single electronic states of Pb adatoms on Pb(111) by means of LT-STM. We observe a clear spatial inhomogeneity within the spectral density of the Pb adatom, which is attributed to the unoccupied orbitals of the Pb adatom. DFT calculations confirm that the Pb adatoms possess sp^3 hybrid atomic orbitals oriented in tetrahedral fashion. In the negative bias regime only the orbital protruding into the vacuum can be detected by the tip, corresponding to a single protrusion. In the positive bias regime the antibonding states possess an asymmetric two-lobe feature, which rotates with the bias voltage in the spatial spectroscopic mapping.

ACKNOWLEDGMENTS

We would like to thank Karl-Heinz Rieder and Shengbai Zhang for helpful discussions. This project is supported partially by the Natural Science Foundation of China (NSFC) (Grants No. 60276041, No. 90406022, No. 60228005, and No. 90201036), Supercomputing Center, CNIC, CAS, and the Volkswagen Foundation Project "Single Molecule Synthesis." W. A. Hofer is supported by the Royal Society.

*hjgao@iphy.ac.cn

[1] F. E. Olsson, M. Persson, A. G. Borisov, J. P. Gauyacq, J. Lagoute, and S. Folsch, Phys. Rev. Lett. **93**, 206803 (2004).
[2] L. Gross, F. Moresco, L. Savio, A. Gourdon, C. Joachim, and K. H. Rieder, Phys. Rev. Lett. **93**, 056103 (2004).
[3] K.-F. Braun and K.-H. Rieder, Phys. Rev. Lett. **88**, 096801 (2002).
[4] A. Yazdani, B. A. Jones, C. P. Lutz, M. F. Crommie, and D. M. Eigler, Science **275**, 1767 (1997).
[5] N. Knorr, M. A. Schneider, L. Diekhoner, P. Wahl, and K. Kern, Phys. Rev. Lett. **88**, 096804 (2002).
[6] P. Wahl, L. Diekhoner, M. A. Schneider, L. Vitali, G. Wittich, and K. Kern, Phys. Rev. Lett. **93**, 176603 (2004).
[7] S. H. Ji, T. Zhang, Y. S. Fu, X. Chen, X. C. Ma, J. Li, W. H. Duan, J. F. Jia, and Q. K. Xue, Phys. Rev. Lett. **100**, 226801 (2008).
[8] D. Kitchen, A. Richardella, J.-M. Tang, M. E. Flatté, and A. Yazdani, Nature (London) **442**, 436 (2006).
[9] T. Risse, S. Shaikhutdinov, N. Nilius, M. Sterrer, and H.-J. Freund, Acc. Chem. Res. **41**, 949 (2008).
[10] N. Nilius, M. V. Ganduglia-Pirovano, V. Brazdova, M. Kulawik, J. Sauer, and H. J. Freund, Phys. Rev. B **81**, 045422 (2010).
[11] G. Binnig and H. Rohrer, Rev. Mod. Phys. **71**, S324 (1999).
[12] J. Tersoff and D. R. Hamann, Phys. Rev. Lett. **50**, 1998 (1983).
[13] G. A. Fiete and E. J. Heller, Rev. Mod. Phys. **75**, 933 (2003).
[14] J. T. Li, W.-D. Schneider, R. Berndt, and B. Delley, Phys. Rev. Lett. **80**, 2893 (1998).
[15] H. C. Manoharan, C. P. Lutz, and D. M. Eigler, Nature (London) **403**, 512 (2000).
[16] V. Madhavan, W. Chen, T. Jamneala, M. F. Crommie, and N. S. Wingreen, Science **280**, 567 (1998).
[17] L. Limot, E. Pehlke, J. Kröger, and R. Berndt, Phys. Rev. Lett. **94**, 036805 (2005).
[18] L. Gross, K.-H. Rieder, F. Moresco, S. M. Stojkovic, A. Gourdon, and C. Joachim, Nature Mater. **4**, 892 (2005).
[19] J. Lagoute, X. Liu, and S. Fölsch, Phys. Rev. Lett. **95**, 136801 (2005).
[20] S. Fölsch, P. Hyldgaard, R. Koch, and K. H. Ploog, Phys. Rev. Lett. **92**, 056803 (2004).
[21] Y. Yayon, V. W. Brar, L. Senapati, S. C. Erwin, and M. F. Crommie, Phys. Rev. Lett. **99**, 067202 (2007).
[22] A. J. Heinrich, J. A. Gupta, C. P. Lutz, and D. M. Eigler, Science **306**, 466 (2004).
[23] N. Nilius, T. M. Wallis, and W. Ho, Phys. Rev. Lett. **90**, 046808 (2003).
[24] J. P. Perdew, J. A. Chevary, S. H. Vosko, K. A. Jackson, M. R. Pederson, D. J. Singh, and C. Fiolhais, Phys. Rev. B **46**, 6671 (1992).
[25] D. Vanderbilt, Phys. Rev. B **41**, 7892 (1990).
[26] G. Kresse and J. Hafner, Phys. Rev. B **47**, 558 (1993).
[27] G. Kresse and J. Furthmüller, Phys. Rev. B **54**, 11169 (1996).
[28] C. M. Wei and M. Y. Chou, Phys. Rev. B **66**, 233408 (2002).
[29] S.-W. Hla, K. F. Braun, V. Iancu, and A. Deshpande, Nano Lett. **4**, 1997 (2004).
[30] S.-W. Hla, K. F. Braun, B. Wassermann, and K.-H. Rieder, Phys. Rev. Lett. **93**, 208302 (2004).
[31] M. Schmid, W. Hebenstreit, P. Varga, and S. Crampin, Phys. Rev. Lett. **76**, 2298 (1996).
[32] Z. H. Cheng, W. H. Soe, W. A. Hofer, H.-J. Gao, and K.-H. Rieder (unpublished).
[33] K. Palotás and W. A. Hofer, J. Phys.: Condens. Matter **17**, 2705 (2005).

[34] W. A. Hofer, Prog. Surf. Sci. **71**, 147 (2003).
[35] F. Silly, M. Pivetta, M. Ternes, F. Patthey, J. P. Pelz, and W. D. Schneider, Phys. Rev. Lett. **92**, 016101 (2004).
[36] J. Repp, F. Moresco, G. Meyer, K. H. Rieder, P. Hyldgaard, and M. Persson, Phys. Rev. Lett. **85**, 2981 (2000).
[37] N. Knorr, H. Brune, M. Epple, A. Hirstein, M. A. Schneider, and K. Kern, Phys. Rev. B **65**, 115420 (2002).